Combining In-situ Measurements, Passive Satellite Imagery, and Active Radar Retrievals for the Detection of High Ice Water Content

Christopher R. Yost, Patrick Minnis, Kristopher M. Bedka, Louis Nguyen, Rabindra Palikonda, Douglas Spangenberg, John Walter Strapp, Julien Delanoë, Alain Protat

▶ **To cite this version:**

Christopher R. Yost, Patrick Minnis, Kristopher M. Bedka, Louis Nguyen, Rabindra Palikonda, et al.. Combining In-situ Measurements, Passive Satellite Imagery, and Active Radar Retrievals for the Detection of High Ice Water Content. AGU Fall Meeting 2016, Dec 2016, San Francisco, United States. pp.A23A-0185. insu-01414794

HAL Id: insu-01414794
https://insu.hal.science/insu-01414794

Submitted on 12 Dec 2016

HAL is a multi-disciplinary open access archive for the deposit and dissemination of scientific research documents, whether they are published or not. The documents may come from teaching and research institutions in France or abroad, or from public or private research centers.

L'archive ouverte pluridisciplinaire **HAL**, est destinée au dépôt et à la diffusion de documents scientifiques de niveau recherche, publiés ou non, émanant des établissements d'enseignement et de recherche français ou étrangers, des laboratoires publics ou privés.

Combining In-situ Measurements, Passive Satellite Imagery, and Active Radar Retrievals for the Detection of High Ice Water Content

Christopher R. Yost[1], P. Minnis[2], K. M. Bedka[2], L. Nguyen[2], R. Palikonda[1], D. A. Spangenberg[1], J. W. Strapp[3], J. Delanoë[4], and A. Protat[5]

A23A-0185

[1]SSAI, Hampton, VA [2]NASA LaRC, Hampton, VA [3]Met Analytics Inc., Ontario, Canada [4]LATMOS/IPSL/UVSQ, Guyancourt, France [5]Bureau of Meteorology, Melbourne, Australia

Introduction

At least one hundred jet engine power loss events since the 1990s have been attributed to the phenomenon known as ice crystal icing (ICI). Ingestion of high concentrations of ice particles into aircraft engines is thought to cause these events, but it is clear that the use of current on-board weather radar systems alone is insufficient for detecting conditions that might cause ICI. Passive radiometers in geostationary orbit are valuable for monitoring systems that produce high ice water content (HIWC) and will play an important role in nowcasting, but are incapable of making vertically resolved measurements of ice particle concentration, i.e., ice water content (IWC). Combined radar, lidar, and in-situ measurements are essential for developing a skilled satellite-based HIWC nowcasting technique. The High Altitude Ice Crystals – High Ice Water Content (HAIC-HIWC) field campaigns in Darwin, Australia; Cayenne, French Guiana; and Ft. Lauderdale, FL, have produced a valuable dataset of in-situ total water content (TWC) measurements with which to study conditions that produce HIWC. The NASA Langley Satellite ClOud and Radiative Property retrieval System (SatCORPS) was used to derive cloud physical and optical properties such as cloud top height, temperature, optical depth, and ice water path from multi-spectral satellite imagery acquired throughout the HAIC-HIWC campaigns. These cloud properties were collocated with the in-situ TWC measurements in order to characterize cloud properties in the vicinity of HIWC. Additionally, a database of satellite-derived overshooting cloud top (OT) detections was used to identify TWC measurements in close proximity to convective cores likely producing large concentrations of ice crystals. Certain cloud properties show some sensitivity to increasing TWC and a multivariate probabilistic indicator of HIWC was developed from these datasets. This paper describes the algorithm development and demonstrates the HIWC indicator with imagery from the HAIC-HIWC campaigns. Vertically resolved IWC retrievals from active sensors such as the Cloud Profiling Radar (CPR) on CloudSat and the Doppler Radar System Airborne (RASTA) provide IWC profiles with which to validate and potentially enhance the satellite-based HIWC indicator.

Acknowledgements

This research was supported by the NASA High Ice Water Content Program. TWC and RASTA datasets are distributed by the NCAR/UCAR Earth Observing Laboratory. CloudSat Standard Data Products are distributed by the CloudSat Data Processing Center located at the Cooperative Institute for Research in the Atmosphere (CIRA) at Colorado State University in Fort Collins.

Overview of HAIC-HIWC Campaigns and Datasets

During the HAIC-HIWC campaigns, in-situ cloud total water content (TWC) was measured by an isokinetic evaporator probe (IKP2; Davison et al. 2012, *AIAA*) mounted to a research aircraft. Satellites in geostationary orbit were relied upon for continuous multi-spectral imagery of storms producing large concentrations of ice particles. A brief summary of the HAIC-HIWC campaigns is provided in the table below including the geostationary satellite imagers that provided coverage for each campaign.

Campaign Location	Dates	Number of Flights	Aircraft	GEO Satellite Coverage
Darwin, Australia	Jan-Mar 2014	23	SAFIRE Falcon-20	MTSAT-1R, MTSAT-2
Cayenne, French Guiana	May 2015	16	SAFIRE Falcon-20	GOES-13, Meteosat-10
Ft. Lauderdale, FL, USA	August 2015	10	NASA DC-8	GOES-13, GOES-14

Cloud property retrievals (e.g., cloud boundaries, optical depth, water path) were derived from satellite imagery using the SatCORPS (Minnis et al. 2011), and an automated overshooting top (OT) detection algorithm (Bedka and Khlopenkov, 2016, *JAMC*) was used to identify locations of cirrus anvils and deep convective updrafts.

The OT detection algorithm is a set of statistical, spatial and frequency analyses of IR and VIS imagery and consists of two main components:

(1) IR-based detection of anvil clouds and brightness temperature (BTW) minima within these regions. OT candidates are assigned an "OT Probability" score.

(2) Quantification of cloud texture in 1-km visible imagery via a unitless rating. Values greater than 5 are indicative of strong vertical motions and gravity waves, and larger values correspond to classic OT "cauliflower-like" texture.

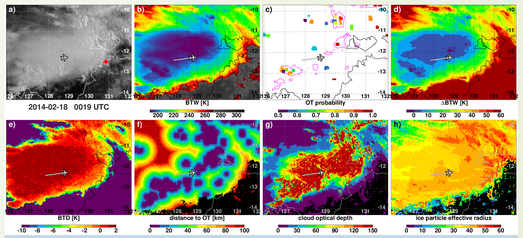

Images (derived from MTSAT-1R) of **(a)** visible reflectance, **(b)** IR window brightness temperature (BTW), **(c)** visible texture rating (magenta contours) and OT probability rating (color shading), **(d)** difference between IR-window and tropopause temperatures (ΔBTW), **(e)** brightness temperature difference between water vapor and IR-window channels (BTD), **(f)**, distance to nearest OT, **(g)** ice cloud optical depth (COD), and **(h)** ice particle effective radius for Darwin flight #22 on 18 February, 2014.

Spatial/temporal collocation of aircraft and satellite data:

Assuming a typical airspeed of 180 m/s, the 1-Hz aircraft measurements were averaged to 45-s intervals in order to approximate the relatively coarse satellite spatial resolution. The four nearest satellite pixels were matched to each segment of the flight tracks and the mean cloud properties were computed. Temporal differences between the observations were restricted to less than 10 minutes. Satellite temporal resolution ranged from 1-minute (GOES-14 imagery for three flights during Florida campaign) to 30-minute (GOES-13 during Cayenne campaign).

Image time and aircraft position on the figure at left correspond to boxed time period (0019 UTC) on time series (right).

TWC is a flight-level measurement. RASTA radar retrievals of IWC typically reveal higher IWC below flight level.

BTD is somewhat indicative of HIWC but remains constant through much of this flight.

HIWC was often encountered in the vicinity of detected OTs.

High COD is also closely associated with HIWC, but reliable retrievals are only available during the day.

Ice particle effective radius exhibits no useful signal for HIWC identification.

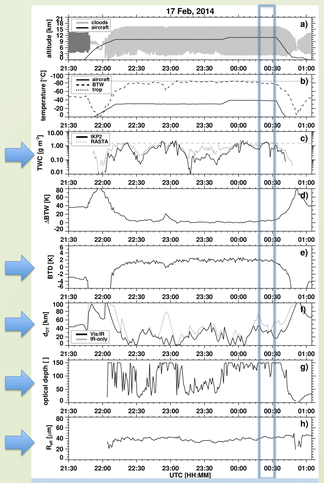

Time series of collocated aircraft and satellite measurements/retrievals for Darwin flight #22 on 17 Feb , 2014.

In-situ Measurements of IWC

No single threshold can delineate HIWC from low IWC (LIWC), but values smaller than 0.25 g m^{-3} are typically not considered high. Values of 0.25 and 1.0 g m^{-3} represent the 48th and 82nd percentiles, respectively, of the TWC* dataset (45-s averages).

Cumulative distribution functions (CDFs) of satellite observations/retrievals were generated for different ranges of TWC (below). Distance from OT (d_{OT}) shows the most potential for distinguishing LIWC from HIWC. Almost all instances of TWC > 1.0 g m^{-3} occurred within ~40 km of evident convection identified by the automated OT detection algorithm.

All other parameters except effective ice particle radius R_{eff} show some ability to distinguish LIWC from HIWC as indicated by the separation between the green and black curves. However, it is difficult to distinguish HIWC from moderate values (small separation between the blue and green curves).

Effective ice particle radius R_{eff} exhibits no skill for distinguishing even very low from very high IWC. IWP is a function of both COD and R_{eff}, so it is preferable to use COD rather than IWP as a HIWC predictor.

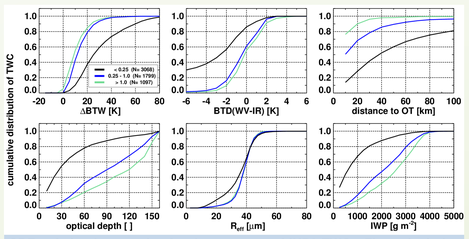

CDFs of cloud properties for three ranges of IKP2 TWC. Figure includes Florida IKP2 draft dataset.

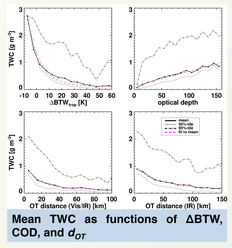

Mean TWC as functions of ΔBTW, COD, and d_{OT}

Mean TWC was computed as a function of ΔBTW, COD, and d_{OT} (left). Since visible texture detection is not available at night, mean TWC was computed as a function of distance from IR-only detections too.

A fuzzy logic method was adopted here for estimating HIWC probability PHIWC) in satellite imagery given ΔBTW, COD, and d_{OT}. Functional fits to mean TWC (left, magenta curves) were used to obtain values ranging 0.0 – 1.0 for each input. Final PHIWC values were obtained by taking the cubic root of the product of the three scores.

TWC and PHIWC trends track especially well with trends in d_{OT}, particularly when the satellite temporal resolution is very high (see time series below). During the Florida campaign, 1-minute imagery was available for three flights (see right time series).

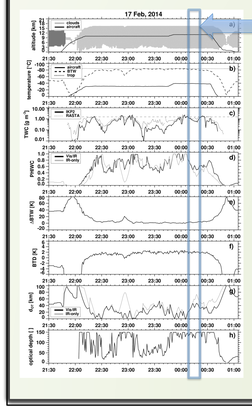

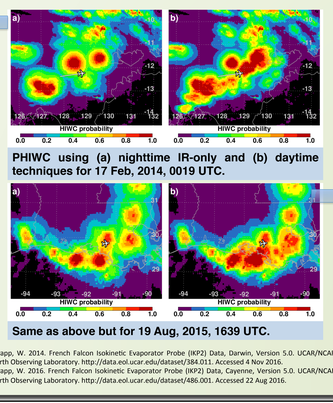

PHIWC using (a) nighttime IR-only and (b) daytime techniques for 17 Feb, 2014, 0019 UTC.

Same as above but for 19 Aug, 2015, 1639 UTC.

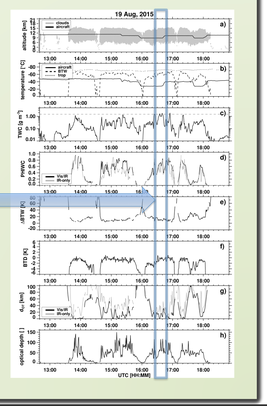

*Strapp, W. 2014. French Falcon Isokinetic Evaporator Probe (IKP2) Data, Darwin, Version 5.0. UCAR/NCAR - Earth Observing Laboratory. http://data.eol.ucar.edu/dataset/384.011. Accessed 4 Nov 2016.

*Strapp, W. 2016. French Falcon Isokinetic Evaporator Probe (IKP2) Data, Cayenne, Version 5.0. UCAR/NCAR - Earth Observing Laboratory. http://data.eol.ucar.edu/dataset/486.001. Accessed 22 Aug 2016.

Radar Measurements of IWC

RASTA** (Doppler Radar System Airborne) is an airborne 95-GHz cloud radar operated on the Falcon-20 during the Darwin and Cayenne campaigns. RASTA radar measurements are capable of providing IWC retrievals for the entire cloud column thus providing a more complete characterization of cloud structure above and below flight level.

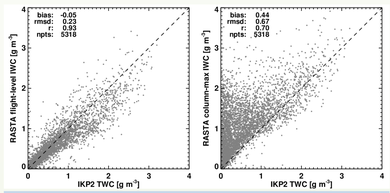

Comparisons of in-situ IKP2 TWC and (left) RASTA flight level and (right) RASTA column-max IWC

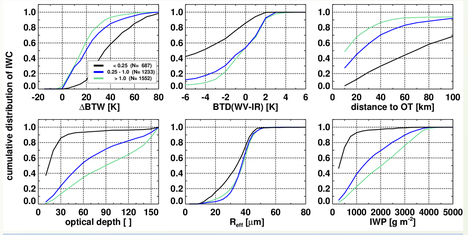

CDFs of cloud properties for three ranges of RASTA column-max IWC

Flight-level IWC from IKP2 and RASTA agree quite well (top, left), but RASTA often reveals higher IWC below flight level (top and bottom right). Very dense clouds may attenuate the radar beam making IWC retrieval impossible, and even higher IWC may exist beneath the level of attenuation.

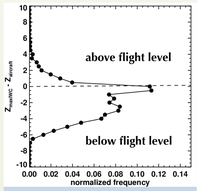

Difference between altitude of max IWC and aircraft flight level

CDFs of cloud properties as functions of RASTA column max IWC (above) show results similar to those obtained with IKP2 TWC (see previous section). Here there is better separation of LIWC and HIWC using COD and IWP. RASTA measurements indicate the presence of HIWC up to 100 km from OT detections.

During the Cayenne campaign there was a coordinated flight with a CloudSat overpass at ~1720 UTC on May 16, 2015. This provided a unique opportunity to compare in-situ measurements with satellite retrievals and to validate HIWC diagnostic products.

Satellite observed fields including PHIWC are shown in the images at right. The CloudSat ground track is shown by the dashed line on each image, and the aircraft track is shown on panel (h). An OT was detected less than 10 km away from the aircraft's position.

Flight level IWC was extracted from the CloudSat 2B-CWC-RO product and compared to in-situ TWC and satellite-estimated PHIWC. Uncertainties in the CloudSat retrievals (gray shading) are rather large for the peak values shown here, but CloudSat IWC retrievals agree well with TWC. PHIWC follows TWC trends well but does not capture the secondary peak in max IWC just south of 4.5°N latitude.

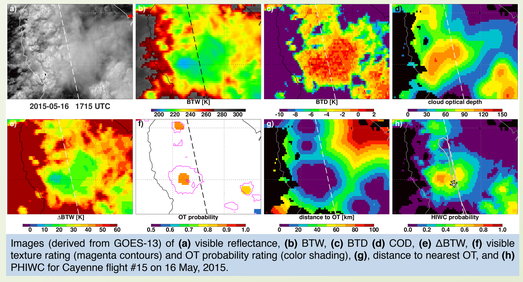

Images (derived from GOES-13) of **(a)** visible reflectance, **(b)** BTW, **(c)** BTD **(d)** COD, **(e)** ΔBTW, **(f)** visible texture rating (magenta contours) and OT probability rating (color shading), **(g)**, distance to nearest OT, and **(h)** PHIWC for Cayenne flight #15 on 16 May, 2015.

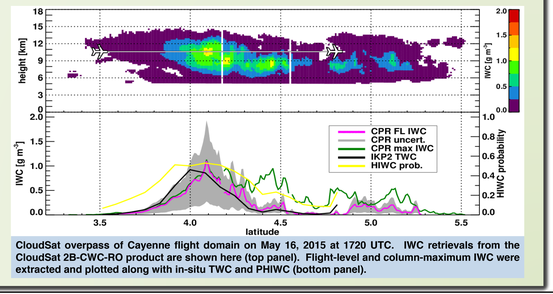

CloudSat overpass of Cayenne flight domain on May 16, 2015 at 1720 UTC. IWC retrievals from the CloudSat 2B-CWC-RO product are shown here (top panel). Flight-level and column-maximum IWC were extracted and plotted along with in-situ TWC and PHIWC (bottom panel).

**Delanoë, J., 2016. Radar Aéroporté et Sol de Télédétection des Propriétés Nuageuses. (RASTA), Version 5.2. Accessed 28 July, 2016.

PHIWC Validation/Verification Methods

Given that "HIWC" is a loosely-defined term, validation of HIWC diagnostic tools is a challenge. "Impulse events" can be minimized by avoiding strong updrafts as previously shown, but exposure of aircraft engines to low or moderate IWC for a long duration is also an important scenario to consider.

PHIWC > 0.6 was obtained for most TWC > 1 g m^{-3} using the fuzzy logic method presented here, but many moderate TWC were also given similar values. ~90% of TWC < 0.25 had PHIWC < 0.6 (top).

Computation of HIWC probability of detection (POD) and false-alarm rates (FAR) are one method for evaluating performance. Receiver-operator characteristic (ROC) curves are a convenient method to display both quantities. POD and FAR are shown here as functions of different PHIWC thresholds used to signify HIWC. Lower thresholds result in higher POD but also higher FAR.

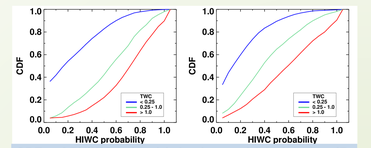

CDFs of PHIWC using (a) daytime and (b) nighttime IR-only methods as functions of TWC.

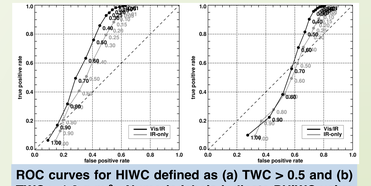

ROC curves for HIWC defined as (a) TWC > 0.5 and (b) TWC > 1.0 g m^{-3}. Numeric labels indicate PHIWC value used to distinguish HIWC from LIWC.

Drastically different POD and FAR are obtained for different definitions of HIWC. High FAR seem inevitable given the significant overlap of HIWC and LIWC statistics.

Summary

High concentrations of ice particles, i.e., HIWC, have been linked to aircraft engine power loss events at cruise altitudes where the existence of supercooled water droplets is extremely improbable.

In-situ ice water content measurements were matched to satellite cloud property retrievals in order to characterize HIWC events from a satellite perspective and develop an algorithm to estimate the probability of high ice water content PHIWC in satellite imagery.

Most HIWC occurred within or near optically thick clouds with significant texture and/or prominent cold spots. There is significant overlap in the distributions of different satellite observations for moderate and high IWC encounters.

PHIWC validation studies highlight the tradeoff between probability of detection and false alarm rates. The HIWC nowcasting community will need to establish a method to effectively validate HIWC diagnostic products.

Next-generation sensors such as the Advanced Baseline Imager (ABI) on GOES-R and the Advanced Himawari Imager (AHI) on Himawari-8 offer the necessary spatial and temporal resolution for studying environments that produce HIWC.